

Behavior of copper-containing high-entropy alloys in harsh metal-dusting environments

Mathias C. Galetz¹  | Clara Schlereth¹  | Emma M. H. White² 

¹Dechema-Forschungsinstitut—High-Temperature Materials, Frankfurt, Germany

²Ames Laboratory Ringgold Standard Institution—Materials Sciences and Engineering, Ames, Iowa, USA

Correspondence

Mathias Galetz, Dechema Forschungsinstitut—High-Temperature Materials, Theodor-Heuss-Allee 25, 60486 Frankfurt, Germany.
Email: galetz@dechema.de and mathias.galetz@dechema.de

Funding information

Office of Energy Efficiency and Renewable Energy, Grant/Award Number: DE-AC02-07CH11358

Abstract

Metal dusting is still an unresolved issue at high temperatures. Currently, two material-related strategies to mitigate metal dusting are described in the literature. On the one hand, highly alloyed materials are used, which contain large amounts of protective oxide-forming elements, such as Cr, Al, and Si. The second mitigation strategy is based on inhibiting the catalytic effect of Fe, Ni, and Co. These elements all strongly catalyze the formation of solid carbon from the gas phase. Combining the catalytic protection of Cu alloying for metal dusting with protection by a classical alumina/chromia barrier is a native feature that high-entropy alloys (HEAs) can offer. In this study, the behavior of different equiatomic HEAs with and without Al and/or Cu are studied when exposed at 620°C in a highly aggressive metal-dusting environment.

KEYWORDS

high-entropy alloys, metal dusting

1 | INTRODUCTION

The processing and storage of energy through the turnover of carbon-containing gases suffer from one of the most critical material corrosion problems at high temperatures. The carbon-rich, thermodynamically unstable gases of such processes induce the extremely aggressive high-temperature corrosion form of “metal dusting.”^[1–3] It occurs in conventional processes of energy technologies and the chemical engineering and petrochemical industry, as well as innovative and new efficient processes, such as dry reforming or co-electrolysis. Metal dusting appears at temperatures ranging from about 400°C to 850°C, with the greatest risk in the range of 600–650°C.^[3,4] It is characterized by high carbon ingress into the material followed by carbide and graphite formation within the microstructure. The graphite formation leads to a strong volume increase and ultimately to disintegrating stresses in the material. The corrosion

usually manifests as local, extremely fast-growing damage in the form of “pits” out of which the dust (“metal dust”) from metal particles, oxides, cementite, graphite, and amorphous carbon grows, which gave this corrosion issue its name. In addition, it is difficult to predict because it often affects only small areas of components, which see the most critical conditions, especially in heat exchangers, as well as on intakes, outlets, transition pieces, and cooler flanges.

Currently, two material-related strategies to mitigate metal dusting are described in the literature. On the one hand, highly alloyed materials are used, which contain large amounts of protective oxide-forming elements, such as Cr, Al, and Si. The durability of these materials under highly carburizing conditions relies on the formation of dense and slow-growing oxide barriers, which protect the base material from the corrosive environment. Examples of such materials include Alloy 602 CA, Alloy 690, Alloy 699 XA, or Alloy 693.^[5–8] In addition, from the class of

This is an open access article under the terms of the Creative Commons Attribution-NonCommercial-NoDerivs License, which permits use and distribution in any medium, provided the original work is properly cited, the use is non-commercial and no modifications or adaptations are made.

© 2021 The Authors. *Materials and Corrosion* published by Wiley-VCH GmbH

high-alloyed steels, the Al_2O_3 -forming Kanthal APMT (Fe-21Cr-5Al-3Mo),^[9] as well as aluminide coatings,^[10] should be mentioned. The second mitigation strategy is based on inhibiting the catalytic effect of Fe, Ni, and Co, which all strongly catalyze the formation of solid carbon from the gas phase.^[1] The alloying elements Sn, Ge, and Cu have the demonstrated capability to catalytically suppress carburization in metal-dusting environments.^[11–13] On the basis of this concept, coatings with Ge and Sn were developed,^[11,14,15] as well as alloys with Cu.^[16–20] Cu was shown to decrease the metal-dusting attack significantly, an effect ascribed to the low solubility for carbon in Cu as well as the inhibition of graphite formation within the alloy. In a study on the metal dusting of binary Ni-Cu alloys, Nishiyama et al.^[19] showed that with a Cu concentration of 20 wt%, the surface reaction is inactivated within the CO-containing synthesis gas and the material is protected from metal dusting. The impact of different Cu levels in austenitic steels was investigated by Zhang and Young,^[16,20] and was shown to improve the alloys' resistance up to a certain content, for example, up to 10 wt% Cu for 310 steel. Above a certain level, depending on the steel grade, a Cu-solid solution phase is precipitated, which leads to deleterious behavior. This is in contrast to binary Ni-Cu alloys, in which the higher the Cu content, the better the performance,^[19] as the binary system shows solubility over the full range of compositions. Two commercial high-temperature materials that have adapted the Cu alloying concept are the Ni-base materials HR-235 and alloy 696 with Cu contents between 2 and 4 wt%. The alloying content is rather low due to the limited alloying capability of Cu in classical multielement, high Cr-containing Ni-base alloys. Unwanted phase formation, embrittlement, and hot cracking can occur, especially during welding with a Cu content of above ~4 wt%.^[21,22] Mn is another element that is believed to strongly affect metal dusting, as—in contrast to Fe, Cu, Co, or Ni—it oxidizes in metal-dusting environments and, therefore, tends to promote unwanted spinel formation with Cr.^[23] However, Mn-containing scales can prevent coking.^[23]

The alloying concept of high-entropy alloys (HEAs) has only recently started to be considered for extreme environments. HEAs were introduced by Yeh and Cantor^[24,25] in 2004, and ever since, many additional HEA systems have been reported. These HEAs are defined as alloys with five or more principal elements with a concentration between 5 and 35 at%.^[26] Due to their unique multielement composition, HEAs possess interesting properties, including high mechanical strength, hardness, and ductility, which have been the subject of numerous publications.^[24,27–32] Among such systems, the Cantor alloy CoCrFeMnNi is the most extensively

studied HEA. The oxidation behavior of this alloy at intermediate temperatures was studied by Holcomb et al.^[33] They reported the long-term oxidation behavior in the air at 650°C and 750°C, which is dominated by the formation of an Mn/Cr oxide scale. Substituting Al and Cu for Mn makes this alloy an ideal candidate for carburizing environments; as discussed earlier, alloying with Al, Cu, and Cr is key to metal-dusting protection. Initial work on the AlCu-CoCrFeNi system with an overlay welding process^[34] showed that Cu modification promoted spallation of the oxide scales at high temperatures, compared to a Cu-free variation. To date, there is no literature data for this system in the metal-dusting environment and temperature range, even though the mechanical properties of such alloys at metal-dusting temperatures are likely more in line than at higher temperatures. In this study, the behavior of different equiatomic HEAs with and without Al and/or Cu are studied when exposed at 620°C in a highly aggressive metal-dusting environment for potential application in the area of energy processing and storage through the turnover of carbon-containing gases.

2 | MATERIALS AND METHODS

Equiatomic alloy (16.67 or 20 at% for each alloying element) buttons were prepared by vacuum arc melting on a water-cooled Cu hearth with a nonconsumable tungsten electrode. Each button was flipped and remelted three times, by which a homogeneous distribution of each element was achieved. The overview and the nomenclature of the compositions in wt% for a better comparison with classical alloys are given in Table 1. Cubic samples with a few millimeters edge length were arc wire cut from these buttons and ground to 800 grit.

For comparison, a reference sample of alloy 800 was also exposed with the nominal composition given in Table 2 in wt%.

Quasi-isothermal exposure tests were carried out at 620°C in a tube furnace. The gas mixture consisted of

TABLE 1 Actual alloy composition of the different HEAs (determined by SEM-EDX)

In wt%	Al	Cu	Co	Cr	Fe	Ni	Mn
HEA-AlCu	8.5	20.1	18.7	16.5	17.7	18.6	-
HEA-Al	10.7	-	23.3	20.6	22.1	23.2	-
HEA-Mn	-	-	21.0	18.5	19.9	20.9	19.6
HEA-Cu	-	22.0	20.4	18.0	19.3	20.3	-

Abbreviations: EDX, energy-dispersive X-ray; HEA, high-entropy alloy; SEM, scanning electron microscopy.

TABLE 2 Alloy 800 composition (wt% as determined by SEM-EDX)

Fe	Ni	Cr	Mn	Si	Ti	Al	Cu
47.3	28.6	20.5	0.9	1.0	0.4	1.1	0.4

Abbreviations: EDX, energy-dispersive X-ray; SEM, scanning electron microscopy.

20% CO–20% H₂–1% H₂O–8% CO₂–51% Ar in vol% with a carbon activity of $a_C = 358$ (calculated as described for the synthesis gas reaction in Reference [35]) and oxygen partial pressure of 1.7e–23 bar (calculated using Fact-sage®) at a system total pressure of 18 atm. Dry gas flows were adjusted by mass flow controllers and mixed before moisturizing. The H₂O content was supplied by a high-pressure pump, mixed with the dry gas, and vaporized. The samples were exposed under carburizing conditions for up to 800 h. A second set of samples was removed after 100 h. The microstructure, scale formation, pitting, and subsurface microstructure were characterized using metallographic and microanalytic methods, such as optical light microscopy (LOM; Leica DLMA) and electron probe microanalysis (EPMA; Jeol JXA-8100). Whenever mean compositions are given, they were derived from an average of at least three spots. X-ray diffraction (XRD) and Raman spectroscopy measurements of the surface were conducted using a Bruker D8 Advance with Co-K α radiation and a Renishaw inVia with a 633-nm laser, respectively.

3 | RESULTS

Although the microstructure is not the main focus of this study, the different phases and microstructures of the different alloys are shown due to their relevance for the corrosion behavior. Figure 1 shows an overview of the different alloys as they appear in the light microscope. Figure 2 additionally shows the diffraction patterns after 400-h exposure.

3.1 | HEA-Mn (CoCrFeMnNi)

This “Cantor alloy” alloy is probably the most investigated HEA. Interestingly, in the as-cast condition, some brighter and darker contrast areas are visible even in the LOM picture (Figure 1), which represents minor Mn segregation of less than 2-at% variation. As confirmed by XRD measurement (Figure 2), the alloy is single-phase. This is in line with the findings of Cantor et al.^[25] as well as other published XRD measurements and neutron diffraction patterns, revealing just one

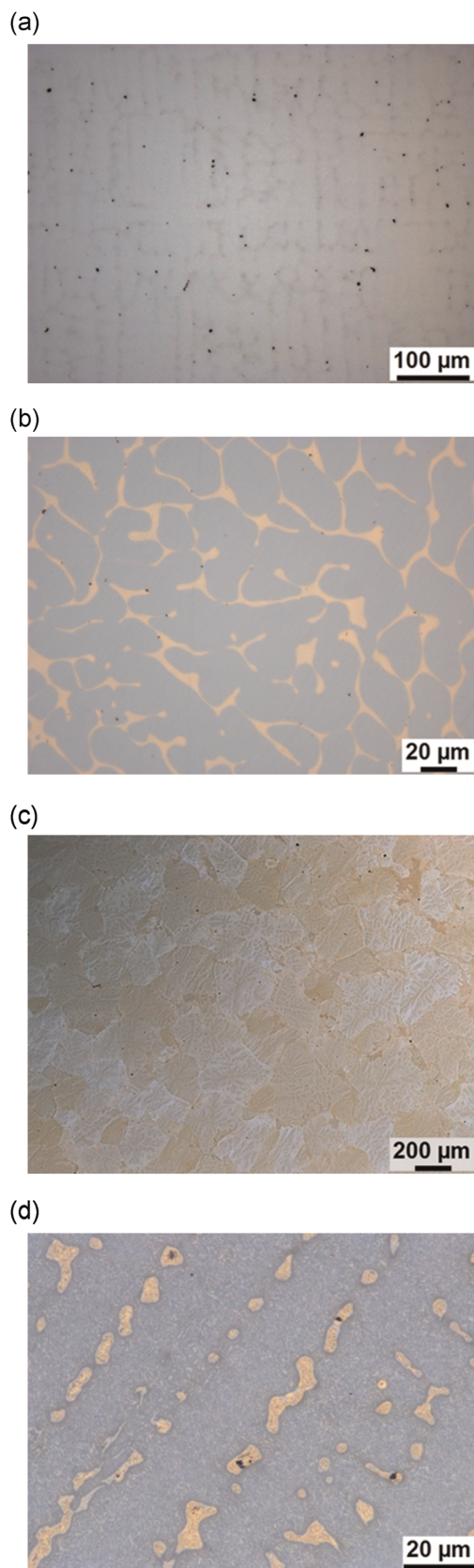


FIGURE 1 Light micrographs of (a) HEA-Mn, (b) HEA-Cu, (c) HEA-Al, and (d) HEA-AlCu alloys (Note the different magnifications chosen to best show certain pronounced features). HEA, high-entropy alloy [Color figure can be viewed at [wileyonlinelibrary.com](https://onlinelibrary.wiley.com/doi/10.1002/maco.202012075)]

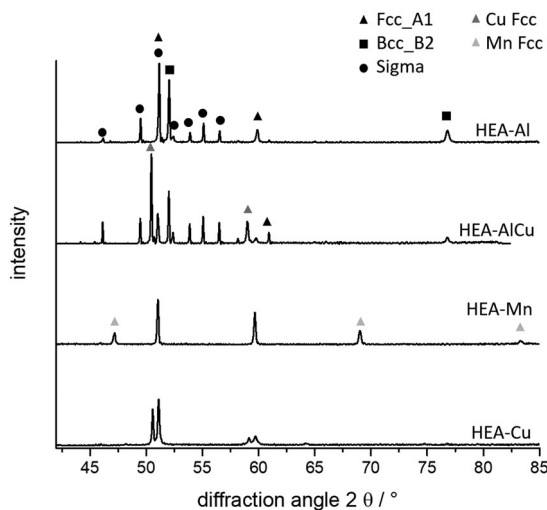


FIGURE 2 Diffraction patterns of the cross-sections of the different high-entropy alloys (HEAs) after 400 h of exposure at 620°C

phase.^[36,37] However, unexpected additional peaks of a second FCC (face-centered cubic) phase with a much larger lattice parameter (indicated as FCC [Mn-rich] in Figure 2) appeared after exposure at 620°C. A similar observation was reported that employed transition electron microscopy (TEM) investigations, suggesting a very small-scale secondary FCC phase, but further examination is beyond the scope of this study.^[37]

3.2 | HEA-Cu (CoCrCuFeNi)

For the alloy in which Mn is substituted by Cu, an interpenetrating network of a Cu-rich (~45 at%) and a Cu-lean (~15 at%) FCC microstructure evolves (see Figures 1b and 2). The presence of this second FCC phase is in line with the ternary Cu-Fe-Ni phase diagram.^[38] In this ternary system, Cu has very limited solubility. For this comparison, Co and Cr are neglected; however, a similar solubility gap occurs in the Cu-Co system,^[39] which, in combination, explains the low Co solubility in the Cu-based FCC phase and, in general, the two-phase FCC microstructure of HEA-Cu, which can be found in the literature as well.^[40]

3.3 | HEA-Al (AlCoCrFeNi)

The HEA-Al alloy is also one of the most commonly investigated HEAs^[41] and solidifies into dendrites and interdendritic regions, as shown in Figure 1c, which was previously observed.^[42] XRD data shows two phases, an Al-rich, Cr-lean (18.8 at% Al/23.7 at% Cr) BCC

(body-centered cubic) phase, and an FCC phase rich in Cr (12.8 at% Al, 29.2 at% Cr), which is in good agreement with a TEM study by Manzoni et al.,^[43] who found that Cr-Fe-rich precipitates are embedded in an Al-Ni-rich matrix. After exposure at 620°C, an additional sigma phase is observed, which is known to be precipitated at the temperature range around 600°C in Cr-rich steels such as AISI 309. On the other hand, sigma-phase precipitation has been minimally described for this alloy system,^[41] with the exception of Sitla et al.,^[44] who did observe a transformation of the Cr-Fe-rich regions into the sigma phase.

3.4 | HEA-AlCu (AlCoCrCuFeNi)

If the alloy is modified with Al and Cu, highly pronounced Cu-rich FCC phase is found in a BCC matrix (compositions in Table 3), which is again in good agreement with the literature.^[45]

For HEA-AlCu exposure at 620°C, again Cr-rich precipitates were indicated by EPMA variations in the Cr signal, and XRD analysis confirmed the presence of sigma phase. Several authors annealed this alloy in the relevant temperature range; however, a lot of data shows significant scattering (which we also observed, when measuring with a Cu-K α) and sigma phase could thus have been easily overlooked. For example, when carefully looking at the XRD patterns in Figure 10 of Reference [45] who annealed Al_{0.5}CoCrCuFeNi at 600°C and 700°C for 10 h, the representative peaks of the sigma-phase can be identified. When reviewing the literature, Ng et al.^[46] is the only reference that describes the sigma phase after annealing between 300°C and 850°C for Al_{0.5}CoCrCuFeNi. On the basis of the Cr-signal in the EPMA, such precipitates are also well below 1 μ m; thus, further TEM studies would be necessary for additional analysis, which is beyond the scope of this corrosion study.

4 | METAL-DUSTING ATTACK

After exposure for 800 h, neither HEA-Al nor HEA-AlCu showed pit formation. After 100-h exposure in the metal-dusting atmosphere, SEM/EDX confirmed that oxygen is

TABLE 3 Phases of HEA-AlCu and their compositions

Phase (at%)	Fe	Cr	Ni	Al	Co	Cu
FCC	5.1	3.5	11.5	13.0	6.0	66
BCC	22.0	23.5	19.9	20.7	20.9	14.8

Abbreviations: BCC, body-centered cubic; FCC, face-centered cubic; HEA, high-entropy alloy.

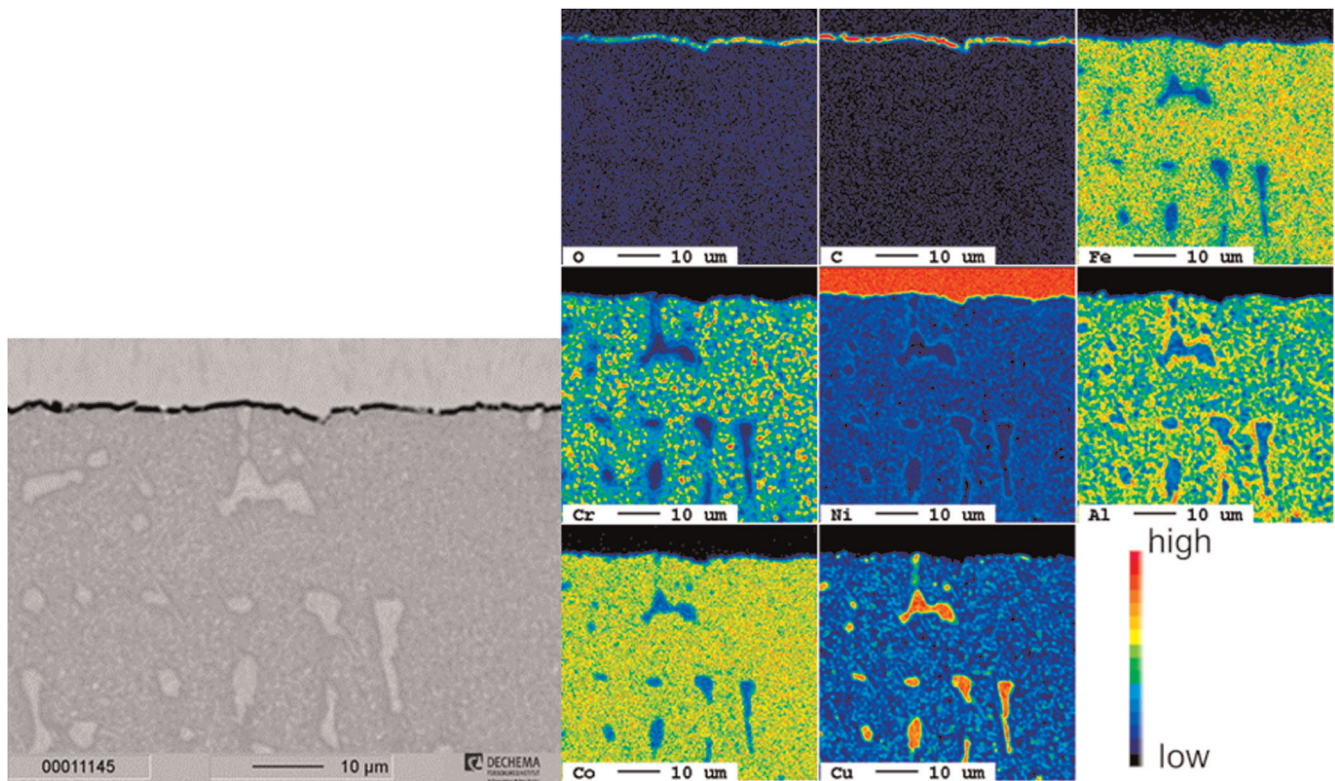


FIGURE 3 Electron probe microanalysis of the cross-section of HEA-AlCu after 400-h exposure. HEA, heat-entropy alloy [Color figure can be viewed at [wileyonlinelibrary.com](https://onlinelibrary.wiley.com/doi/10.1002/maco.202012075)]

enriched at the surface, as well as Cr and Al. These results prove the selective oxidation of such elements at the surface to form a scale, which acts as a barrier for carbon ingress. Both scales on the Al-containing HEAs are very thin in the range of $\sim 1 \mu\text{m}$ (see Figure 3, representing the EPMA of the HEA-AlCu alloy). The sample was Ni-plated to protect the oxide scale during preparation, which does not prevent carbon uptake from the embedding resin into the cracks and pores of the oxide scale. The metals that form the oxide scale are not easily visible in Figure 3 because it is so thin. However, what can be seen are the small Cr-rich precipitates, which were determined to be sigma-phase by XRD.

This slow-growing behavior of the oxide can be explained easily by Raman investigation (Figure 4), which shows the typical twin-peak that belongs to α -alumina, which is formed on both alloys. After 100 h, the peak already appears for the HEA-AlCu alloy and its location at about 1400 cm^{-1} suggests alumina. However, after 400 h, it evolves into a distinct twin peak. The HEA-Al alloy shows the same clear α -alumina signal, which is exemplified in Figure 4 for the signals after 400-h exposure.

When the surfaces after 400 h of exposure are compared for HEA-Al, many very fine needles (with a length of 100–200 nm) are visible (Figure 5a), whereas, for HEA-AlCu, fewer slightly thicker needles are visible (not

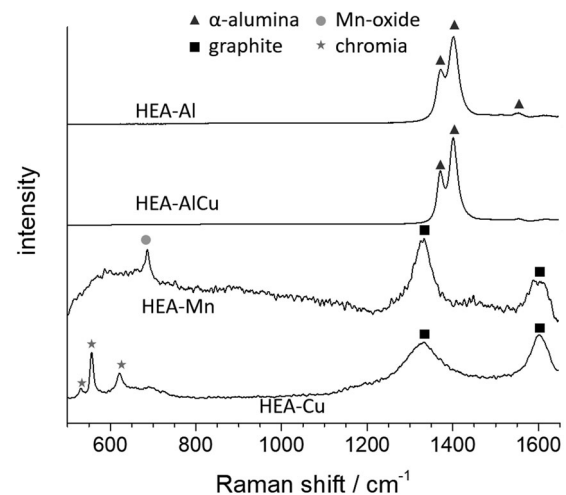


FIGURE 4 Raman spectra of HEA-Al and HEA-AlCu after 800-h exposure as well as of HEA-Mn and HEA-Cu after 400-h exposure. HEA, heat-entropy alloy

shown). As identifying α -alumina at these temperatures is quite surprising, additional samples were investigated by SEM after 100 exposures only (Figure 5b,c). After this rather short exposure time and low temperature, crystal needles were not yet visible on the HEA-Al alloy, whereas for the HEA-AlCu, needles can already be seen in

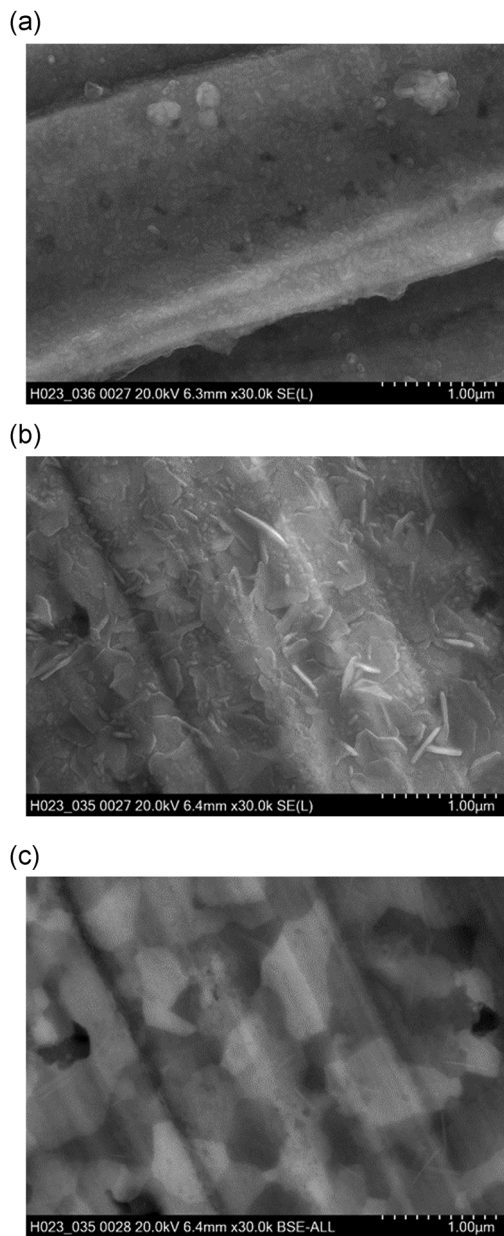


FIGURE 5 Top view of the oxide scale of HEA-Al using the SE detector (a) and HEA-AlCu by SE (b) and BSE (c) after 100 h. BSE, backscattered electron; HEA, high-entropy alloy; SE, secondary electron

the SEM. For the HEA-AlCu alloy, the Cu-rich phase can still be seen in backscattered electron (BSE) mode through the scale (not shown), which allowed a comparison with the secondary electron picture and revealed needles are evident on the surface of both phases with no clear difference between them. Such needles are usually a good indication of the formation of metastable alumina and show that Cu alloying impacts the alumina scale formation on such alloys, but the Cu mechanism of influence is not clear. The finding of α -alumina after exposure at 620°C for a few hundred hours is surprising, as, usually metastable alumina

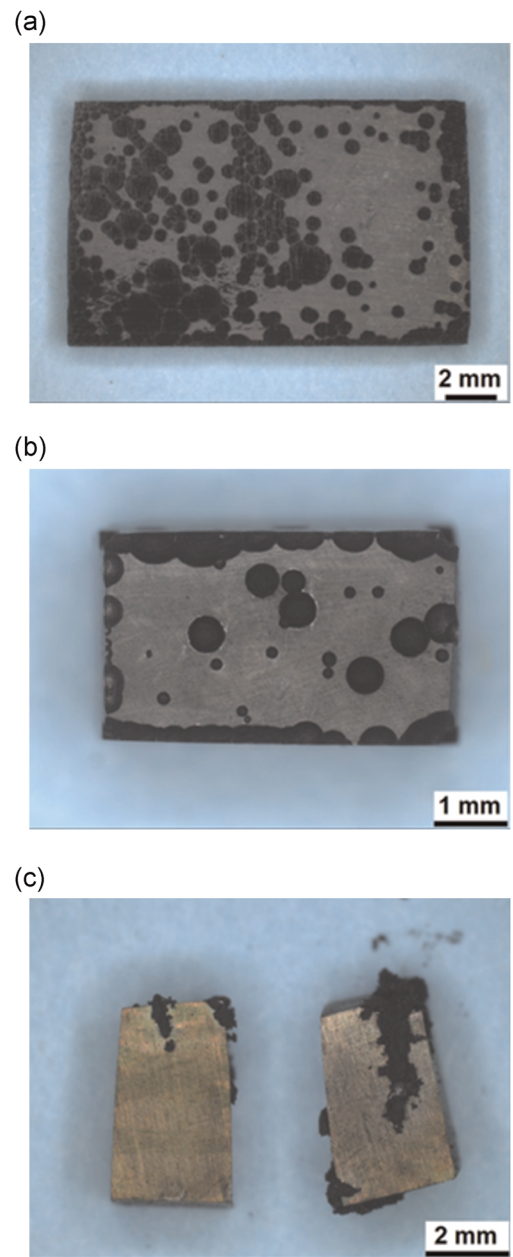


FIGURE 6 (a) Alloy 800 after 300 h, (b) HEA-Mn after 400 h, and (c) HEA-Cu after 400 h. HEA, high-entropy alloy [Color figure can be viewed at wileyonlinelibrary.com]

is found when Al oxidizes, such as a γ - or θ - Al_2O_3 , and α -alumina is often reported to be limited to much higher oxidation temperatures (above 900°C).^[47] Though additional oxides, such as Cr_2O_3 and TiO_2 , can both enhance corundum formation,^[48] 620°C is very low and might be related to the specific composition of the HEA, in combination with the low oxygen partial pressure and thus low oxide growth rates, allowing time for α -alumina nucleation. Though this finding guarantees excellent resistance in metal-dusting environments, the exact mechanism should be phenomenologically investigated in the future.

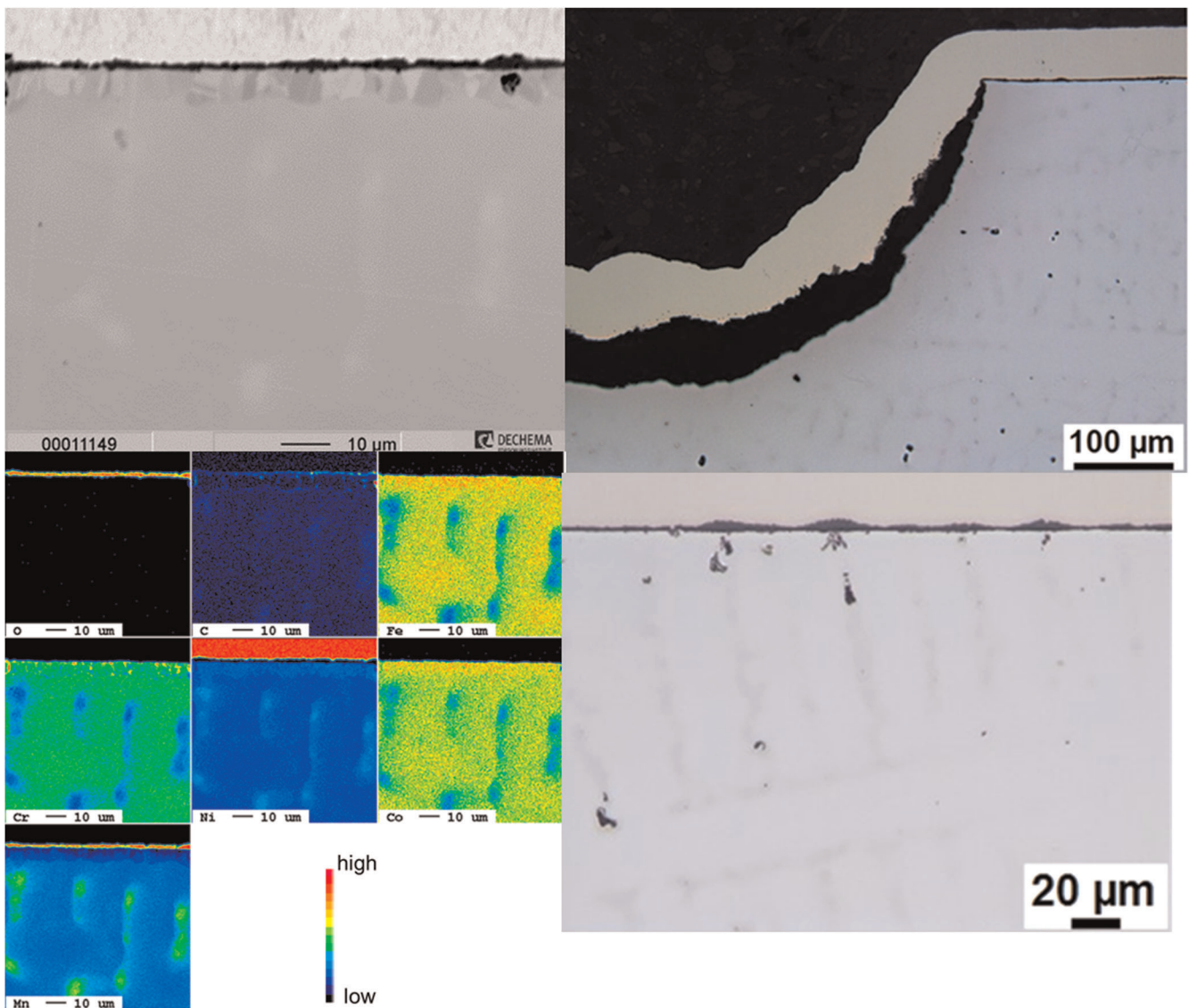


FIGURE 7 Electron probe microanalysis of the alloy HEA-Mn after exposure showing Mn segregation (element distribution, left) and several pits (exemplified, upper right) and internal oxidation and accelerated oxide growth in the Mn-rich regions [Color figure can be viewed at [wileyonlinelibrary.com](https://onlinelibrary.wiley.com/terms-and-conditions)]

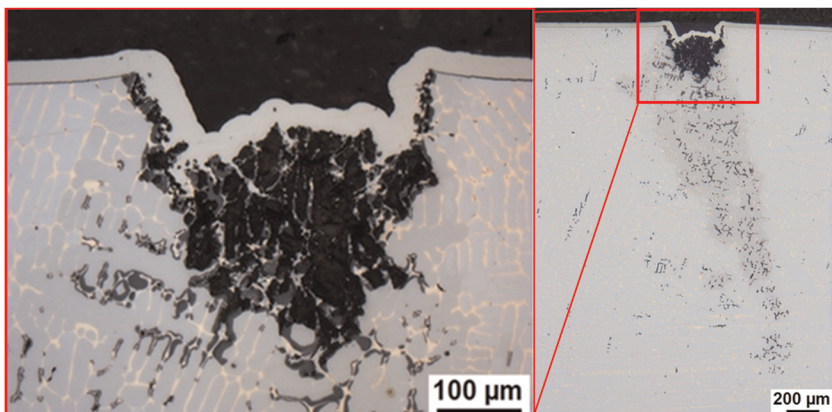


FIGURE 8 Attack on HEA-Cu in areas, which do not form a thin oxide scale. HEA, high-entropy alloy [Color figure can be viewed at [wileyonlinelibrary.com](https://onlinelibrary.wiley.com/terms-and-conditions)]

In contrast to the Al-containing HEAs, Alloy 800, HEA-Mn, and HEA-Cu were severely attacked after 300 or 400 h, respectively, as shown in Figure 6, and had to be removed from the test due to massive coke production.

Interestingly, for the three alloys that showed metal dusting, the attack manifests differently. Alloy 800, as

well as HEA-Mn, show classical round-shaped pits, as shown in Figures 6a and 6b, respectively. Alloy 800 is well known to be a chromia former in metal-dusting environments at 620°C,^[4] but Fe- and Mn-spinel can occur, lowering its protective properties in comparison to Ni-based alloys. The HEA-Mn alloy formed an almost pure outer Mn oxide/spinel-scale (see Raman signal in

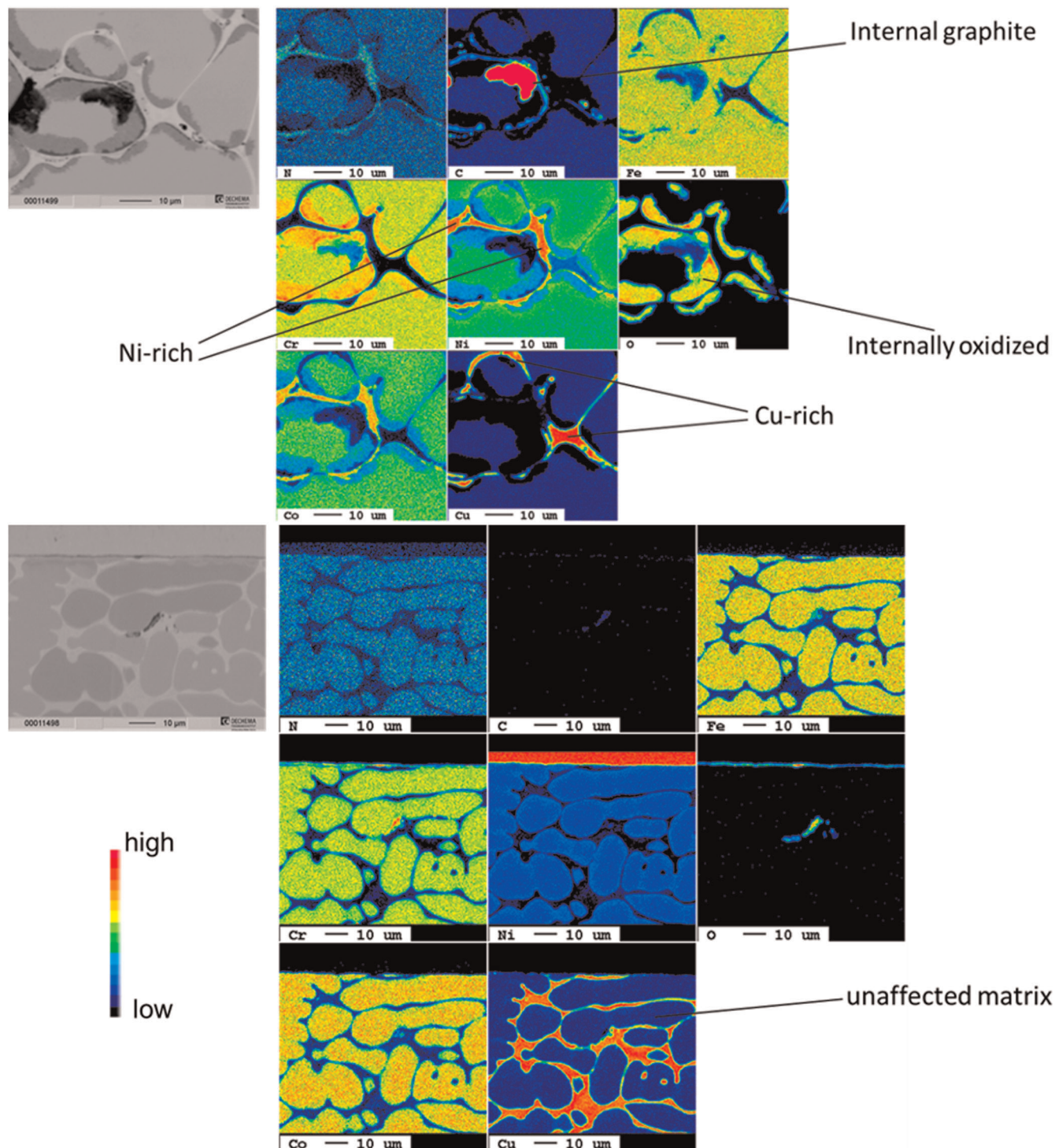


FIGURE 9 Electron probe microanalysis of the microstructure of significantly (under pit) and lightly affected zones of the alloy HEA-Cu. HEA, high-entropy alloy [Color figure can be viewed at [wileyonlinelibrary.com](https://onlinelibrary.wiley.com)]

Figure 4), which is reflected by an about 10- μm -thick depletion zone (Figure 7a). Extensive Mn-oxide formation was also observed by Holcomb et al.^[33] when the Cantor alloy was oxidized at 650°C in the air.

After the metal-dusting exposure, the outer Mn spinel is visible in the cross-section, where the scale locally thickened and internal oxidation is present. Such localized thickening can be linked to the Mn-rich segregation in the subsurface zone and might be ideal incubation sites for pit formation due to the formation of less protective oxides. Though that seems a reasonable assumption, the difficulty is that the body of evidence (Mn) is always consumed quickly as soon as pit formation starts. The pits themselves show the round shape typical for metal dusting (Figure 7), as can also be seen when compared to Alloy 800 in Figure 6. In contrast to the HEA-Mn alloy, the alloy HEA-Cu exhibits a much thinner scale and mainly consists of chromia, as shown by Raman analysis (Figure 4). As can be seen in Figure 6, in a large area fraction of the alloy, this chromia scale is capable of protecting the alloy, which confirms the positive results found in the literature for the Cr-Cu combination to prevent metal dusting.^[16] However, with scale failure, the pit close to the surface of the material disintegrates and only a little Cu-rich metal residue is left (Figure 8).

Exacerbating this effect, when the scale fails on the HEA-Cu alloy, the attack is much stronger than for the other HEAs. Not only do the pits have a less regular shape, clearly affected by the two-phase microstructure, but also the attack propagates deeply into the material (Figure 8). The results of EPMA of the samples exposed for 400 h are shown in Figure 9 for the HEA-Cu in a zone underneath the pit and an unaffected region, respectively.

Underneath the pit and deeper within the material, internal oxidation of chromia is found along the phase boundaries of the Cu-rich FCC phase. Interestingly, in such Cr-depleted zones, carbon also locally precipitated around the Cu-rich phase. Both Cr and C seem to diffuse along the phase boundaries of the Cu-rich phase and are disrupting the material. This preferential attack at the phase boundaries was also observed^[16] for 304, 310, and alloy grades, which were alloyed with 20 at% Cu and also formed large amounts of Cu-rich phase. However, certain differences are visible between the steels' microstructure and HEA systems after exposure to metal-dusting environments. In steels, precipitated carbides were found within the alloys. Instead, in the HEA-Cu, no carbides were found and oxygen was the main reactant that first diffused inwards along the phase boundaries of the Cu-rich phase. Over time in such areas, where Cr, C, and O already led to internal chromia formation and carbon precipitation along with a change within the

TABLE 4 Phase compositions (at%) observed in the area where internal oxidation and carbon are present

In at%	C	Fe	Cr	Ni	O	Co	Cu
Unaffected matrix	1.8	23.1	22.7	20.2	0.0	22.7	9.5
Internally oxidized region	1.5	16.5	19.7	10.1	41.1	9.9	1.2
Internal graphite	73.3	3.0	6.5	1.6	13.1	2.3	0.1
Ni/Co-rich	4.5	20.2	2.0	37.4	0.3	31.6	3.9
Cu-rich	3.5	2.6	1.1	11.2	0.6	3.4	77.6

microstructure. In the direct surroundings of the carbon precipitates, the former Cu-rich network separates into zones of almost pure Cu and zones highly enriched in Co and Ni. Initially, the Cu-rich FCC phase contains about 80 at% Cu, with 8 at% Ni and minor other elements. The matrix instead dissolves only 9.5 at% Cu and is almost equiatomic in Co, Ni, Fe, and Cr. Table 4 provides EPMA spot analyses of the different areas after exposure.

In the area of the attack, the matrix composition changes where Cr is internally oxidized and thus depleted from the alloy. What is more surprising is that simultaneously less Co and Ni are present within the matrix, but only in such spots where the internal graphite is also precipitated. The Co and Ni enrich in the originally Cu-rich network that is in contact with the carbon precipitates, combining to form about 70 at% of the metallic phases in this part of the FCC-phase network. At the same time, the Cu signal decreases from an initial amount of 80 at% to only about 4 at% (!). Such diffusion processes triggered by carbon precipitation in the internally oxidized and carburized regions have, to our best knowledge, not been observed before. The Cu instead enriched in other parts of the former Cu-rich, homogeneous FCC network. This change in the microstructure penetrates several millimeters under what can be considered a pit close to the surface, and could potentially cause fast component failure.

5 | CONCLUSIONS

Combining the catalytic protection by Cu alloying for metal dusting with protection by a classical alumina/chromia barrier is a native feature that HEA alloys can offer. However, when the scale fails and an interpenetrating network of Cu-rich phase is present, as is for equiatomic HEA-Cu, the phase boundaries open up fast diffusion paths for oxygen and carbon, inducing a very strong metal-dusting attack. In the HEA-Cu alloy, very interesting interdiffusion phenomena were observed, which suggests that carbon cannot

precipitate in contact with the Cu-rich FCC matrix. Instead, graphite presence will induce redistribution of the alloying element concentrations with the withdrawal of Cu from the areas of graphite precipitation. In agreement with the work of Zhang et al.^[16] for steels, in HEAs, the Cu needs to be restricted to amounts where it does not lead to a Cu-FCC phase in the microstructure for beneficial metal-dusting performance. The Cantor alloy, here denoted as HEA-Mn, also does not show protective behavior and is attacked by pit formation that is typical for metal dusting.

It was demonstrated that Al-containing HEAs possess a high potential for energy processing and storage applications with carbon-containing gases. Both HEA-Al and HEA-AlCu were shown to be α -alumina formers under the investigated conditions and thus fully protect the alloy from metal dusting. In such cases, their particular alloying concept can be highly beneficial. Finally, both alloys with Al precipitated sigma phase, observable after 400 h of exposure at 620°C. Its influence on mechanical properties and scale formation (when Cr is locally bound) needs to be addressed in the future.

ACKNOWLEDGMENTS

The authors would like to thank Susann Rudolphi for the preparation of the cross-sections and Dr. Gerald Schmidt for conducting the EPMA measurements. The authors would also like to thank Dr. Iver Anderson for helpful discussions and the Materials Preparation Center, especially Arne Swanson, at Ames Laboratory for producing the samples. Samples manufactured under funding from the U.S. Department of Energy, Energy Efficiency and Renewable Energy, Advanced Manufacturing Office through Ames Laboratory Contract DE-AC02-07CH11358.

DATA AVAILABILITY STATEMENT

Data available on request.

ORCID

Mathias C. Galetz  <http://orcid.org/0000-0001-6847-2053>

Clara Schlereth  <https://orcid.org/0000-0002-5770-782X>

Emma M. H. White  <https://orcid.org/0000-0002-0246-6256>

REFERENCES

- [1] D. J. Young, J. Zhang, C. Geers, M. Schütze, *Mater. Corros.* **2011**, 62, 7.
- [2] P. A. Lefrancois, W. B. Hoyt, *Corrosion* **1963**, 19, 360.
- [3] R. Schneider, E. Pippel, J. Woltersdorf, S. Strauß, H. J. Grabke, *Steel Res.* **1997**, 68, 326.
- [4] Y. Nishiyama, K. Kitamura, N. Otsuka, *Mater. Sci. Forum* **2008**, 595-598, 649.
- [5] D. Röhnert, M. Schütze, T. Weber in *Corros. 2007 Conf. Expo.*, NACE, Nashville, TN **2007**, p. 7417.
- [6] A. Rouaix-Vande Put, K. A. Unocic, M. P. Brady, B. A. Pint, *Corros. Sci.* **2015**, 92, 58.
- [7] B. A. Baker, G. D. Smith, V. W. Hartmann, L. E. Shoemaker, S. A. McCoy in *Corros. 2002*, NACE, Denver, CO **2002**.
- [8] C. G. M. Hermse, H. van Wortelin *Proc. Eurocorr 2008, Edinburgh*, DECHEMA e.V, Frankfurt am Main, Germany **2008**.
- [9] J. N. Olovsson, D. Chandrasekaran, F. Rave in *8th Int. Symp. High-Temp. Corr. Protect. Mater.*, Les Embiez, France **2012**.
- [10] A. Agüero, I. Baráibar, R. Muelas, C. Oskay, M. Galetz, E. Korner, *Int. J. Press. Vessel. Pip.* **2020**, 186, 104129.
- [11] C. Geers, M. Schütze, *ECS Trans.* **2009**, 25, 71.
- [12] M. A. A. Motin, P. R. Munroe, D. J. Young, M. P. Brady, *Scr. Mater.* **2007**, 56, 281.
- [13] J. Zhang, D. M. I. Cole, D. J. Young in *Proc. EFC Worksh.*, Luleå University of Technology, Luleå, Sweden **2004**.
- [14] S. Madloch, M. C. Galetz, C. Geers, M. Schütze, *Surf. Coat. Technol.* **2016**, 299, 29.
- [15] S. Madloch, M. C. Galetz, *Surf. Coat. Technol.* **2017**, 315, 335.
- [16] J. Zhang, D. J. Young, *Corros. Sci.* **2007**, 49, 1450.
- [17] J. Zhang, M. Safarzadeh, D. J. Young, *Oxid. Met.* **2008**, 70, 15.
- [18] J. Zhang, D. J. Young, *Corros. Sci.* **2012**, 56, 184.
- [19] Y. Nishiyama, K. Moriguchi, N. Otsuka, T. Kudo, *Mater. Corros.* **2005**, 56, 806.
- [20] A. Fabas, D. Monceau, C. Josse, P. Lamesle, A. Rouaix-Vande Put, *Corros. Sci.* **2016**, 107, 204.
- [21] F. F. Noecker, J. N. DuPont, *J. Mater. Sci.* **2007**, 42, 510.
- [22] S. Rao, A. Y. Al-Kawaha, *Weld. J.* **2010**, 89, 46.
- [23] Y. S. Chung, H. Kim, H. C. Yoon, J. S. Chung, N. M. Sammes, *Fuel Cells* **2015**, 15, 416.
- [24] J.-W. Yeh, S.-K. Chen, S.-J. Lin, J.-Y. Gan, T.-S. Chin, T.-T. Shun, C.-H. Tsau, S.-Y. Chang, *Adv. Eng. Mater.* **2004**, 6, 299.
- [25] B. Cantor, I. T. H. Chang, P. Knight, A. J. B. Vincent, *Mater. Sci. Eng. A* **2004**, 375, 213.
- [26] M.-H. Tsai, J.-W. Yeh, *Mater. Res. Lett.* **2014**, 2, 107.
- [27] C.-J. Tong, M.-R. Chen, J.-W. Yeh, S.-J. Lin, S.-K. Chen, T.-T. Shun, S.-Y. Chang, *Metall. Mater. Trans. A* **2005**, 36, 1263.
- [28] A. V. Kuznetsov, D. G. Shaysultanov, N. D. Stepanov, G. A. Salishchev, O. N. Senkov, *Mater. Sci. Eng. A* **2012**, 533, 107.
- [29] Y. J. Zhou, Y. Zhang, F. J. Wang, G. L. Chen, *Appl. Phys. Lett.* **2008**, 92, 241917.
- [30] Y. J. Zhou, Y. Zhang, Y. L. Wang, G. L. Chen, *Appl. Phys. Lett.* **2007**, 90, 181904.
- [31] M. A. Hemphill, T. Yuan, G. Y. Wang, J. W. Yeh, C. W. Tsai, A. Chuang, P. K. Liaw, *Acta Mater.* **2012**, 60, 5723.
- [32] Y. Zhang, X. Yang, P. K. Liaw, *JOM* **2012**, 64, 830.
- [33] G. R. Holcomb, J. Tylczak, C. Carney, *JOM* **2015**, 67, 2326.
- [34] X. Ye, M. Ma, Y. Cao, W. Liu, X. Ye, Y. Gu, *Phys. Procedia* **2011**, 12, 303.
- [35] D. J. Young, *High-Temperature Oxidation and Corrosion of Metals*, Elsevier, Oxford, UK **2008**.
- [36] K. Zhang, Z. Fu, *Intermetallics* **2012**, 28, 34.
- [37] W. H. Liu, Y. Wu, J. Y. He, Y. Zhang, C. T. Liu, Z. P. Lu, *JOM* **2014**, 66, 1973.
- [38] P. Villars, A. Prince, H. Okamoto, *Handbook of Ternary Alloy Phase Diagrams*, ASM International, Materials Park, OH **1997**.

- [39] T. Nishizawa, K. Ishida, *Bull. Alloy Phase Diagr.* **1984**, 5, 161.
- [40] N. Park, I. Watanabe, D. Terada, Y. Yokoyama, P. K. Liaw, N. Tsuji, *Metall. Trans. A* **2015**, 46, 1481.
- [41] C. Zhang, F. Zhang, H. Diao, M. C. Gao, Z. Tang, J. D. Poplawsky, P. K. Liaw, *Mater. Des.* **2016**, 109, 425.
- [42] Y. P. Wang, B. S. Li, M. X. Ren, C. Yang, H. Z. Fu, *Mater. Sci. Eng. A* **2008**, 491, 154.
- [43] A. Manzoni, H. Daoud, R. Völkl, U. Glatzel, N. Wanderka, *Ultramicroscopy* **2013**, 132, 212.
- [44] H. R. Sistla, J. W. Newkirk, F. Frank Liou, *Mater. Des.* **2015**, 81, 113.
- [45] C.-W. Tsai, M.-H. Tsai, J.-W. Yeh, C.-C. Yang, *J. Alloys Compd.* **2010**, 490, 160.
- [46] C. Ng, S. Guo, J. Luan, S. Shi, C. T. Liu, *Intermetallics* **2012**, 31, 165.
- [47] M. A. Trunov, M. Schoenitz, X. Zhu, E. L. Dreizin, *Combust. Flame* **2005**, 140, 310.
- [48] Y. Kitajima, S. Hayashi, T. Nishimoto, T. Narita, S. Ukai, *Oxid. Met.* **2011**, 75, 41.

How to cite this article: Galetz MC, Schlereth C, White EMH. Behavior of copper-containing high-entropy alloys in harsh metal-dusting environments. *Materials and Corrosion*. 2021;72:1232–1242.
<https://doi.org/10.1002/maco.202012075>